Application of High-Resolution 1H MAS NMR Spectroscopy to the Analysis of Intact Bones from Mice Exposed to Gamma Radiation

Authors: Zhang, Qibin, Hu, Jian Zhi, Rommereim, Donald N., Murphy, Mark K., Phipps, Richard P., et al.

Source: Radiation Research, 172(5) : 607-616

Published By: Radiation Research Society

URL: https://doi.org/10.1667/RR1715.1

RADIATION RESEARCH **172**, 607–616 (2009)
0033-7587/09 $15.00

DOI: 10.1667/RR1715.1

Application of High-Resolution ^{1}H MAS NMR Spectroscopy to the Analysis of Intact Bones from Mice Exposed to Gamma Radiation

Qibin Zhang,[a] Jian Zhi Hu,[a,1] Donald N. Rommereim,[a] Mark K. Murphy,[a] Richard P. Phipps,[b] David L. Huso[c] and John F. Dicello[c,d]

[a] *Pacific Northwest National Laboratory, Richland, Washington 99352;* [b] *University of Rochester School of Medicine and Dentistry, Lung Biology and Disease Program and Department of Environmental Medicine, Rochester, New York 14642;* [c] *Johns Hopkins University, School of Medicine, Baltimore, Maryland 21205; and* [d] *Department of Radiation Medicine, Loma Linda University Medical Center, Loma Linda, California 92354*

Zhang, Q., Hu, J. Z., Rommereim, D. N., Murphy, M. K., Phipps, R. P., Huso, D. L. and Dicello, J. F. Application of High-Resolution ^{1}H MAS NMR Spectroscopy to the Analysis of Intact Bones from Mice Exposed to Gamma Radiation. *Radiat. Res.* 172, 607–616 (2009).

Herein we demonstrate that high-resolution magic angle spinning (MAS) ^{1}H NMR can be used to profile the pathology of bone marrow rapidly and with minimal sample preparation. The spectral resolution obtained allows several metabolites to be analyzed quantitatively. The level of NMR-detectable metabolites in the epiphysis + metaphysis sections of mouse femur were significantly higher than that observed in the diaphysis of the same femur. The major metabolite damage to bone marrow resulting from either 3.0 Gy or 7.8 Gy of whole-body γ radiation 4 days after exposure were (1) decreased total choline content, (2) increased fatty acids in bone marrow, and (3) decreased creatine content. These results suggest that the membrane choline phospholipid metabolism (MCPM) pathway and the fatty acid biosynthesis pathway were altered as a result of radiation exposure. We also found that the metabolic damage induced by radiation in the epiphysis + metaphysis sections of mouse femur was higher than that of the diaphysis of the same femur. Traditional histopathology analysis was also carried out to correlate radiation damage with changes in metabolites. Importantly, the molecular information gleaned from high-resolution MAS ^{1}H NMR complements the pathology data.

INTRODUCTION

Humans can be exposed to various kinds of ionizing radiation, including the diagnostic X rays, nuclear medicine and radiotherapy routinely used in clinics, radionuclides such as radon, potassium, uranium and nuclear waste, radiological weapons, and high-energy particle radiation from galactic and solar cosmic rays (*1*). All cells can be damaged by ionizing radiation, but actively dividing cells are more radiosensitive than cells that are neither meiotically nor mitotically active (*2*). Bone marrow stem cells are among the most radiosensitive cells in the human body. Ionizing radiation impairs hematopoiesis through a variety of mechanisms. Radiation exposure directly damages hematopoietic stem cells and alters the capacity of bone marrow stromal elements to support and/or maintain hematopoiesis. Exposure to radiation induces dose-dependent declines in circulating hematopoietic cells not only through reduced bone marrow production but also by the redistribution and apoptosis of mature formed elements of the blood (*3–7*).

Magnetic resonance imaging (MRI) is widely used for clinical diagnosis of bone marrow malignancies (*8–11*). However, MRI is useful mainly for detecting malignancies when tumors have already reached a relatively large size, e.g., a few hundred micrometers or more depending on the sensitivity of the spectrometer and the methods used, and thus it is not an effective method for early diagnosis. Since biochemical changes in the diseased tissues precede tumor formation, early diagnosis could be achieved if information could be obtained at the molecular level. In principle, detailed information about biochemical changes in the bone marrow can be provided by high-resolution NMR methods through *ex vivo* analysis of chemical extracts of marrow (*12, 13*). The *ex vivo* process usually starts with either crushing the bone into small pieces or flushing the marrow out with saline, followed by lysing the cells and extracting the cell lysate with organic solvents. Then standard high-resolution liquid-state NMR can be used to analyze the extracted molecular entities. Although impressive spectral resolution can be obtained, standard *ex vivo* methods involve extensive sample preparation and are therefore prone to artifacts induced by incomplete sample extraction, fractionation and sample degradation during this lengthy process.

Like solids, tissues and cells cannot be analyzed directly by standard liquid-state NMR spectroscopy due

[1] Address for correspondence: Pacific Northwest National Laboratory, Richland, WA 99352; e-mail: Jianzhi.Hu@pnl.gov.

to the line broadenings induced by residual static dipolar interactions, residual chemical shift anisotropy interactions, and, most importantly, the variation of local magnetic-field gradients at the compartment boundaries in cells and tissues (*14, 15*). However, when the sample is spun about an axis at the magic angle (54°44′) and a sample spinning rate of several kHz or more is used, all of these line broadenings can be effectively averaged out, resulting in a high-resolution ^{1}H NMR spectrum. High-resolution MAS ^{1}H NMR has been applied successfully to analyze intact cells and tissues from the brain, lung, kidney, heart and muscle, etc. (*16–21*). With high-resolution MAS, high spectral resolution approaching liquid-state NMR has been achieved. The major advantage of high-resolution MAS ^{1}H NMR over other methods for tissue samples is that there is minimal sample preparation and thus fewer artifacts and better correlation with *in vivo* techniques. As a result, high-resolution MAS ^{1}H NMR has been applied in neuropathology to quantify disease biomarkers in unprocessed brain tissue (*16*). Although high-resolution MAS ^{1}H NMR has been applied successfully to various tissues (*14, 16, 19–24*), to our knowledge there is no information on using high-resolution MAS ^{1}H NMR to obtain biochemical information about the bone marrow in intact bones, where line broadening is particularly significant due to the large magnetic susceptibility variations between the bone and the marrow.

In this study, the effects of radiation on the metabolic profiles of bone marrow in mice exposed to γ radiation were explored using high-resolution MAS ^{1}H NMR on unprocessed bone. In parallel, standard histopathological analysis was used to correlate the histology in bone marrow with the results obtained from the NMR investigations.

MATERIALS AND METHODS

Whole-Body γ Irradiation and Sample Collection

Seven-week-old female C57BL/6 mice were purchased from the Jackson Laboratory (Bar Harbor, ME). After acclimation for 1 week at the animal facility of Pacific Northwest National Laboratory (PNNL), they were randomly assigned to groups of four each. Mice were exposed to whole-body γ radiation using a high-activity source (1250 keV ^{60}Co) with an LET in the range of 0.2–2 keV/μm. For the irradiations, the animals were isolated in the corner of their polymer cages, placed a minimum of 100 cm from the collimated 6000 Ci (222 TBq) ^{60}Co source, and irradiated. After irradiation the isolation barrier was removed and animals were transferred to PNNL Animal Facility. The γ-radiation field at the position of the mice was measured beforehand using a reference-class ionization chamber that was calibrated at the National Institute of Standards and Technology. The resulting absorbed dose rate at a depth of approximately 600 mg/cm^2 was 0.83 Gy/min relative to tissue. Groups of mice were exposed to doses of 0 (control), 3.0 and 7.8 Gy. At 4 and 11 days after exposure, mice were killed humanely with 70/30 CO_2/O_2, and the right femur from each mouse was immediately removed, frozen in liquid N_2, and stored at −80°C until NMR analysis. The left femur from each mouse was prepared for histology study (see below). All animal work was approved by the Institutional Animal Care and Use Committee (IACUC) at PNNL.

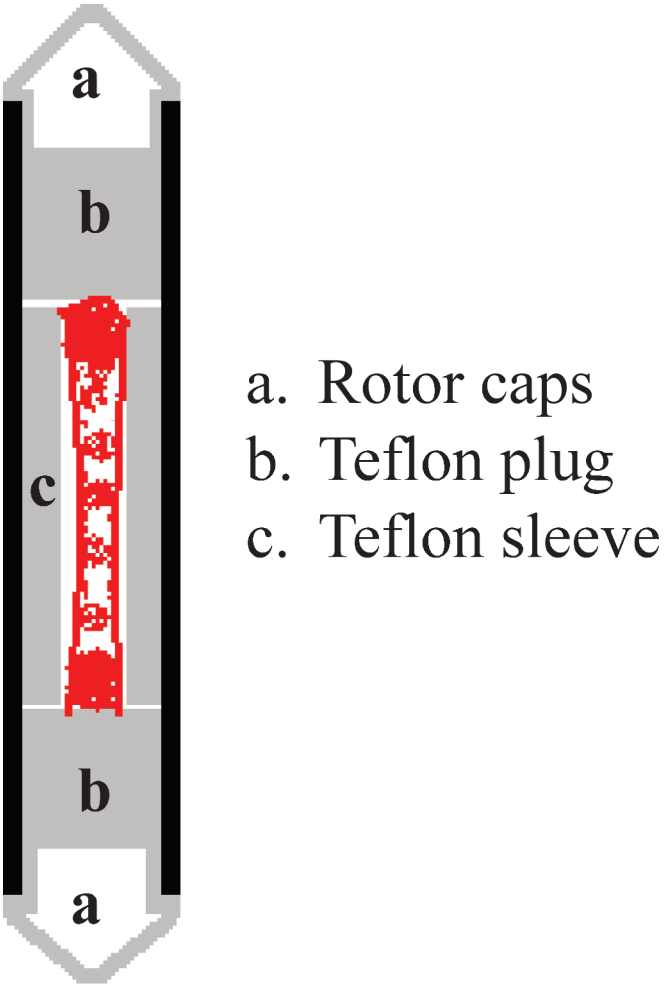

FIG. 1. Schematic of the special liquid-tight sample cell for ^{1}H MAS NMR experiments with mouse femur. The femur was inserted into a Teflon sleeve and closed tightly with two Teflon plugs inside the zirconium sample rotor.

Histopathology Studies

Immediately after excision, the left femur from each mouse was fixed in 10% neutral buffered formalin for histopathological analysis using well-established methods (*25, 26*). Briefly, formalin-fixed femurs were demineralized in formic acid solution, washed, processed in an automated processor, embedded in paraffin, sectioned at 5 μm, mounted on glass microscope slides, and stained with hematoxylin and eosin. The slides were examined by light microscopy.

High-Resolution MAS ^{1}H NMR Measurements

To prepare samples for high-resolution MAS ^{1}H NMR, the left femur was thawed slightly, and outside surrounding tissues were removed under magnification. The whole femur was weighed and inserted into a Teflon tube. The Teflon tube assembly was then loaded between two Teflon plugs in a 7.5-mm-outside-diameter, 6-mm-internal-diameter Chemagnetics pencil rotor as shown in Fig. 1. The two solid Teflon plugs can be inserted into the rotor only by precooling the plugs in liquid nitrogen. In this way, a tight seal is created when the plugs warm to the targeted experimental temperature of 2°C. As a result, the marrow spun at the fast sample spinning

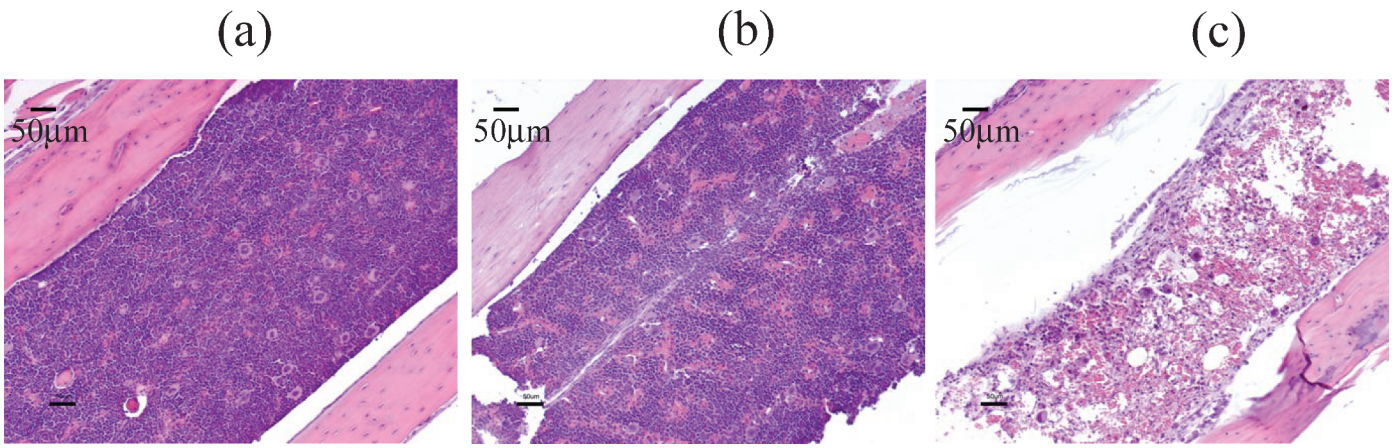

FIG. 2. Histology of mouse femurs, illustrating bone marrow hematopoietic cell depletion at high radiation dose. Panel a: Nonirradiated control mouse; panel b: 4 days after whole-body exposure to 3.0 Gy γ radiation; panel c: 4 days after whole-body exposure to 7.8 Gy.

rate remains inside the sample chamber with no fluid leakage. No fluid leakage was found in more than 100 experiments on femurs using this setup at a sample spinning rate of 4 kHz. In other experiments, femurs with the surrounding tissue removed were also dissected into two sections. One section was a combination of epiphysis (mainly the two femoral heads) and the metaphysis (a short portion of proximal femur beneath the head) while the other section was diaphysis (most of the shaft of the femur). The sample was loaded using the same procedures as for the whole femur.

All ^{1}H NMR experiments were performed at 2°C on a Varian-Chemagnetics 300 MHz Infinity spectrometer operating at a proton Larmor frequency of 299.97 MHz. A standard Chemagnetics CP/MAS probe with a 7.5-mm pencil-type spinner system was used in all the measurements. The sample spinning rate of 4.0 kHz was controlled automatically by a Chemagnetics MAS speed controller at an accuracy of 1 Hz. Temperature was controlled by a Chemagnetics temperature controller in combination with an FTS heating unit. A rotor-synchronized Carr-Purcel-Meibom-Gill pulse sequence, $[90^\circ\text{-}(\tau\text{-}180^\circ\text{-}\tau)_n\text{-acquisition}]$, was used for acquiring data with a total length of 12.5 ms for the echo segment. The 90° pulse length was adjusted for each sample individually and varied from 6.8 to 7.6 μs. The water suppression segment used in this study was a DANTE (delays alternating with nutations for tailored excitation) sequence (*27*) consisting of 6000 small tip angle pulses that were separated by 100 μs. A total of 1920 accumulations were acquired with a total acquisition time of ~1 h for each experiment. The strong lipid $(CH_2)_n$ signal at 1.28 ppm in each spectrum was used as the internal chemical shift reference.

Quantification and Statistical Analysis

The spectrum was integrated with respect to different metabolite peaks in the range of 0.5–4.5 ppm for quantitative data analysis. For comparison within each sample, the integrated peak intensity for each type of metabolite was compared to the most abundant lipid $(CH_2)_n$ peak located at 1.28 ppm in the same spectrum. For comparison between treatment groups, the integrated peak intensity for each type of metabolite in the irradiated group was compared with the same one in the age-matched control group. The reliability of this intertreatment group comparison was validated by performing 12 independent ^{1}H MAS experiment on a 65-mg PBS + 3 m*M* TSP sample during a period of 4 days. For each measurement, the probe was removed from and reinserted into the magnet and the 90° pulse was calibrated. Defining the mean value of the integrated intensity for the TSP peak as 100, the mean ± SD was 100 ± 3. This small standard deviation (3%) indicated that both the spectrometer, including the MAS probe, and the pulse sequence were remarkably stable. Therefore, the integrated metabolite peak intensities from the spectra samples that were acquired under similar experimental conditions could be compared directly.

The statistical significance of differences between the metabolite peak intensities of the exposed group and those of the control group was determined using the Student's *t* test. We used a sample size of four. Furthermore, the *t* test works under the assumption of a Gaussian distribution of data but also works well for distributions that are not Gaussian (*28*).

RESULTS

Histopathology Findings

Typical examples of the cell depletion in bone marrow are shown in Fig. 2. Depletion is defined as a decrease in nucleated cells, which have dark blue nuclei when stained with hematoxylin. The depleted marrow has increased numbers of red blood cells that are not nucleated when mature. Thus the color of the depleted marrow cells appears less basophilic, lighter and more eosinophilic (orange) in Fig. 2c. This indicates that there are fewer basophilic nucleated cells, more white adipose cells, and more eosinophilic non-nucleated erythrocytes.

It is evident from Fig. 2 that there was a mild depletion of hematopoietic cells in the bone marrow of C57BL/6 mice at 4 days after irradiation with 3 Gy (Fig. 2b). By day 11 the bone marrow had returned to a normal histology (not shown). However, the bone marrow was severely depleted at 4 days after exposure to 7.8 Gy (Fig. 2c). The bone marrow cavity contains hematopoietic cells, bone marrow stromal and adipose cells, and bone-forming cells such as osteoblasts and osteoclasts. In the studies shown in Fig. 2, the effects on hematopoietic cells were apparent, while the effects on other cellular components were not.

The Effect of High-Resolution MAS ^{1}H NMR on Whole Femur

A typical example of the effect of MAS on the ^{1}H NMR spectral resolution of a whole femur is shown in

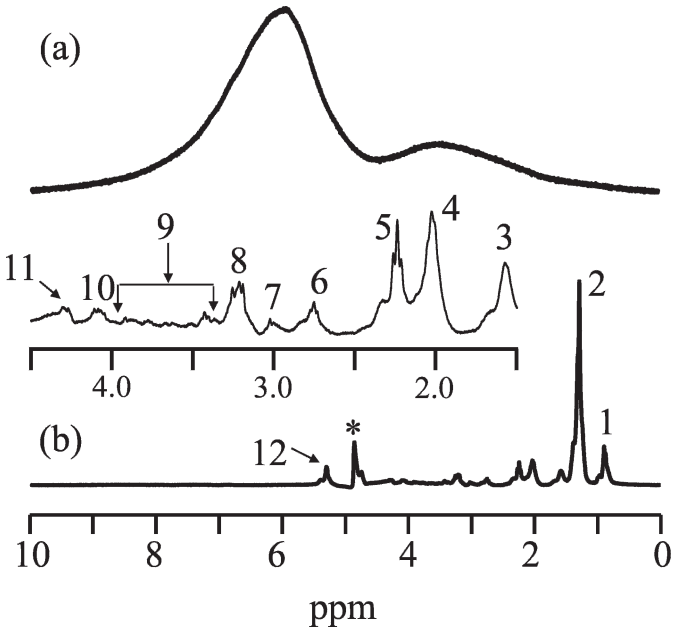

FIG. 3. ^{1}H NMR spectra (300 MHz) of mouse femur acquired at 2°C. (a), Static spectrum; (b), MAS at 4.0 kHz. The assignments of the peaks are as follows: 1, terminal –C**H**$_3$; 2, –(C**H**$_2$)$_n$; 3, –O–CO–CH$_2$–C**H**$_2$–; 4, –CH=CH–C**H**$_2$–CH$_2$–; 5, –O–CO–C**H**$_2$–CH$_2$–; 6, –CH=CH–C**H**$_2$–CH=CH-; 7, creatine; 8, total cholines, including choline, phosphocholine and phosphatidylcholine; 9, glycogen/glucose; 10 and 11, C1, C3-glycerol ester; and 12, –C**H**=C**H**–. The peak in (b) labeled with an asterisk is the residual water signal. The spectrum above to shows the spectral region between 1.5 and 4.5 ppm that is expanded from the spectrum in (b) by about 2.6× horizontally and 5.5× vertically.

Fig. 3. Both the static (Fig. 3a) and the MAS spectra (Fig. 3b) were obtained on the same femur sample and were acquired using the same experimental parameters except that a sample spinning rate of 4 kHz was used in spectrum b. The data presented in Fig. 3a were acquired first, followed immediately by acquisition of those presented in Fig. 3b.

In the static spectrum shown in Fig. 3a, the water peak is so broad that its tail covers a chemical shift range from about 0 to 10 ppm. This is due to the strong magnetic susceptibility variations between the marrow tissue and the bones. As a result, it is impossible to achieve good water suppression without suppressing the corresponding metabolite signals. This prohibits the identification of biologically meaningful metabolites. However, by spinning the sample at 4 kHz (Fig. 3b), water suppression using the same experimental parameters as those in Fig. 3a becomes efficient, and the intensity of the residual water peak at about 4.8 ppm is less than that of the lipid peak at 1.28 ppm. The MAS also greatly enhances the spectral resolution. As shown in Fig. 3b and its corresponding expanded (both horizontally and vertically) insertion spectrum between 1.5 and 4.5 ppm, a number of distinct metabolite peaks were obtained with a narrow peak width. The chemical identities of these major metabolite peaks were assigned according to the published literature (*14, 17, 22–24*) and were labeled on the spectrum. The effect of spinning at 4 kHz on the sample was also tested; there was no visible difference in the spectrum when the sample was respun at 4 kHz (data not shown). In addition, there was no observable difference when the measurement was repeated a few hours after the first measurement (data not shown), showing that there is minimal sample degradation at the experimental temperature of 2°C used throughout this work.

Metabolic Difference between Diaphysis and Epiphysis + Metaphysis Sections

The spectrum in Fig. 4a was acquired on the diaphysis of a femur from the control group, and the spectrum in Fig. 4b was acquired on the epiphysis + metaphysis sections of the same femur. Both spectra were acquired using the same experimental parameters except that the 90° pulse width was calibrated individually.

The femurs of C57BL/6 mice exposed to 3.0 and 7.8 Gy of γ radiation were analyzed as outlined above; i.e., the diaphysis and the epiphysis + metaphysis of the femur were measured separately with high-resolution MAS ^{1}H NMR. Typical spectra for irradiated samples are shown in Fig. 4c–f. Quantitative results obtained from statistical analysis of the high-resolution MAS ^{1}H NMR spectra are summarized in Tables 1 and 2.

For the control groups, the relative ratio of the NMR peaks for the diaphysis and the epiphysis + metaphysis sections of the same femur was significantly different (Table 1). For example, there was a distinct difference in the weight-averaged total peak area between 0.7–4.4 ppm on both day 4 and day 11. High-resolution MAS ^{1}H NMR is unique for selectively assessing the mobile molecules in tissues. Large molecules such as proteins and rigid phospholipids that form the lipid bilayers of healthy cell membranes are essentially invisible to high-resolution MAS ^{1}H NMR if the sample spinning rate used is less than about 6 kHz (*29*). These results clearly showed that the epiphysis + metaphysis contains more mobile molecules than the diaphysis. A careful examination revealed that the increase in the lipid (CH$_2$)$_n$ signal at 1.28 ppm is the main cause for the increased weight-averaged peak area of the epiphysis + metaphysis relative to the diaphysis. This was further confirmed by the data in Table 1 showing the peak areas for the lipid (CH$_2$)$_n$ signal at 1.28 ppm, integrated over a spectral range between 1.1 and 1.4 ppm for the control group, for the diaphysis and the epiphysis + metaphysis at both day 4 and day 11. These results indicate unambiguously that the epiphysis + metaphysis contain more mobile lipids. It can also be seen in the vertically expanded spectral regions between 1.5 and 4.5 ppm in Fig. 4 and the data in Table 2 that for the control mice, higher content of lipid moieties (peaks corresponding to 0.7–1.0, 1.4–1.8 and 1.8–2.15 ppm, mainly the fatty acyl

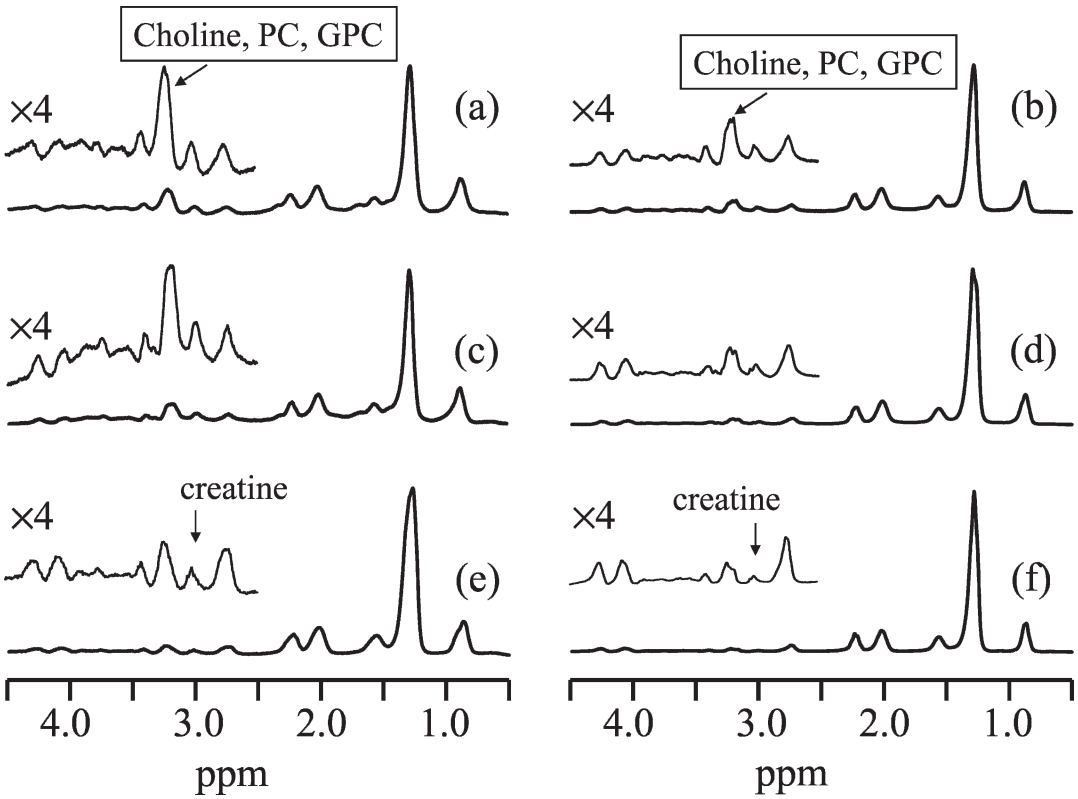

FIG. 4. ^{1}H NMR spectra (300 MHz) of C57BL/6 mouse femurs exposed to 3 and 7.8 Gy whole-body γ radiation. The spectra were acquired at 2°C with MAS at 4.0 kHz. (a) and (b), Controls; (c) and (d), 4 days after exposure to 3 Gy radiation; (e) and (f), 4 days after exposure to 7.8 Gy. (a), (c) and (e) were acquired on the diaphysis of femur while (b), (d) and (f) were acquired on the epiphysis + metaphysis. The diaphysis samples and the epiphysis + metaphysis samples were always from the same three femurs. All the spectral traces are plotted with the lipid signal at 1.28 ppm at the same height to facilitate the comparison. The insertions above each spectrum show the spectral range between 2.5 and 4.5 ppm that is expanded vertically four times.

groups from triglycerides) and total cholines (choline, phosphocholine and phosphatidylcholine at 3.1–3.3 ppm) were observed in the diaphysis compared with the epiphysis + metaphysis. Similar results were obtained from the irradiated groups. These results indicate that the composition of the lipids in the diaphysis is different from that in the epiphysis + metaphysis, i.e., with increased $–CH_3$, $O–CO–CH_2–$, and $–CH=CH–CH_2–$ functional groups accompanied by an increased amount of total cholines. The relative increases in methyl, carboxyl and unsaturated bonds presumably mean that the lipids in the diaphysis contain shorter saturated $(CH_2)_n$ chains compared to the epiphysis + metaphysis. Selective assessment of mobile lipids is important because it has been suggested that mobilization of fatty acids plays an important role in the development of cancer (*30*), obesity and type II diabetes (*31, 32*). Note that mobile lipids are observed in high-resolution MAS ^{1}H NMR at a sample spinning rate while the rigid membranes are not. Therefore, high-resolution MAS ^{1}H NMR can be considered as a selective observation for mobile lipids. The information obtained by high-resolution MAS ^{1}H NMR complements the standard lipid analysis of cell extractions (*33*), in which all of the fatty acids from the cells including cell membranes are analyzed. The lack of similar region-specific histological changes suggests that high-resolution MAS ^{1}H NMR may represent a novel and sensitive means to assess subtle or early events in bone marrow pathology directly in whole bone specimens.

Impact of Radiation on the Epiphysis + Metaphysis of the Femur

After exposure to 3.0 Gy, the integrated peak area for the most abundant lipid peak centered at 1.28 ppm (1.1–1.4 ppm) showed a nonsignificant increase at both 4 and 11 days after irradiation. However, the peak area was statistically significantly increased at 4 days after exposure to 7.8 Gy radiation. The increased lipid signal at the high radiation dose indicates that radiation changed the lipid profile in the epiphysis + metaphysis of the femur. This conclusion was further supported by the weight-averaged total peak area, which was significantly increased both at 4 days after exposure to 7.8 Gy radiation and at 11 days after exposure to 3.0 Gy radiation.

At 4 days after exposure, the relative integrated peak area for total choline (3.1–3.3 ppm), a combination of

TABLE 1
Quantification of the Metabolite Peaks from the Diaphysis (the shaft) and the Epiphysis + Metaphysis (the two heads) of Femurs Excised from Female C57BL/6 Mice Exposed to Gamma Radiation

	Diaphysis of femur				
Treatment group	Control	3.0 Gy	7.8 Gy	Control	3.0 Gy
Days after exposure	4	4	4	11	11
Average weight (mg)	19.2 ± 0.6	19.6 ± 1.9	20.7 ± 0.9*	16.1 ± 1.3	18.5 ± 1.1*
Weight averaged total peak area (0.7–4.4 ppm)	86 ± 8	74 ± 7	162 ± 91	62 ± 13	71 ± 15
Peak area 1.1–1.4 ppm	522 ± 31	513 ± 130	1660 ± 1062	282 ± 122	437 ± 130

Notes. Weight-averaged peak area was calculated by the sum of all the peak areas between 0.7 and 4.4 ppm relative to the weight of the measured femur section. The reported value of peak area, directly proportional to the metabolite concentration in the sample, is referenced to a common fixed spectrometer standard. Four animals were used in each group. Statistically significant differences between the irradiated samples and the corresponding control samples of the same sections are indicated by * for $P < 0.05$. Statistically significant differences between the epiphysis + metaphysis and the diaphysis sections of the same femur are indicated by † for $P < 0.05$ and †† for $P < 0.01$.

choline, phosphocholine and glycerol phosphocholine in the epiphysis + metaphysis of the femur decreased significantly (see the expanded insertion spectra shown in Fig. 4b–d). At 11 days after exposure to 3.0 Gy radiation, the level of total choline in the epiphysis + metaphysis of the femur remained significantly deceased compared with that of the corresponding controls.

For the epiphysis + metaphysis, the relative peak area of creatine (2.9–3.1 ppm) followed a similar trend as that of total choline (Table 2). At 4 days postirradiation, the level of creatine decreased significantly. At 11 days after exposure to 3 Gy, creatine was decreased compared with the corresponding age-matched controls. Creatine is the end product associated with the cellular energy pathway (*17*). The decreased level of creatine suggests that the basic energy pathway was affected by whole-body exposure to γ radiation.

For the epiphysis + metaphysis, the relative ratios for all other peaks remained approximately the same at 4 days after exposure to 3 Gy ($P > 0.05$). However, at 11 days after irradiation, statistically significant decreases were observed for many of the peaks (Table 2), indicating that the effect of radiation increased at longer times.

Effect of Radiation on the Diaphysis of the Femur

As in the epiphysis + metaphysis, 4 days after exposure to 7.8 Gy radiation, there were statistically significant decreases in the relative areas of all the peaks (Table 2) for the diaphysis compared with the corresponding controls. However, in contrast to the results obtained for the epiphysis + metaphysis of the femur, there were no significant differences in total choline and creatine 4 days after exposure to 3 Gy radiation. Furthermore, at 11 days postirradiation, except for the peaks corresponding to the terminal methyl groups (0.7–1.0 ppm) and the –CH=CH–C**H**$_2$–CH$_2$–(1.8–2.15 ppm) groups, there were no significant differences for any of

TABLE 2
Within-Sample Summary of the Metabolic Profiling Results from the Diaphysis and Epiphysis + Metaphysis of Femurs Excised from Female C57BL/6 Mice Exposed to Gamma Radiation

	Diaphysis				
Treatment group	Control	3 Gy	7.8 Gy	Control	3 Gy
Days after exposure	4	4	4	11	11
0.7–1.0 ppm	0.36 ± 0.07	0.33 ± 0.05	0.20 ± 0.03**	0.43 ± 0.08	0.31 ± 0.04*
1.1–1.4 ppm	1.00 ± 0.08	1.00 ± 0.25	1.00 ± 0.64	1.00 ± 0.43	1.00 ± 0.30
1.4–1.8 ppm	0.24 ± 0.03	0.23 ± 0.03	0.17 ± 0.02**	0.25 ± 0.02	0.25 ± 0.03
1.8–2.15 ppm	0.34 ± 0.07	0.31 ± 0.04	0.20 ± 0.03**	0.42 ± 0.07	0.32 ± 0.04*
2.15–2.4 ppm	0.22 ± 0.02	0.22 ± 0.03	0.16 ± 0.02**	0.267 ± 0.03	0.22 ± 0.02
2.5–2.9 ppm	0.12 ± 0.02	0.10 ± 0.02	0.08 ± 0.01*	0.14 ± 0.02	0.12 ± 0.02
2.9–3.1 ppm	0.10 ± 0.04	0.08 ± 0.02	0.03 ± 0.02*	0.13 ± 0.03	0.11 ± 0.03
3.1–3.3 ppm	0.27 ± 0.09	0.20 ± 0.06	0.06 ± 0.03**	0.325 ± 0.11	0.24 ± 0.07
3.3–3.5 ppm	0.08 ± 0.02	0.08 ± 0.05	0.03 ± 0.02**	0.12 ± 0.03	0.09 ± 0.03
3.5–4.2 ppm	0.36 ± 0.11	0.31 ± 0.11	0.15 ± 0.07*	0.49 ± 0.13	0.33 ± 0.09
4.2–4.4 ppm	0.09 ± 0.02	0.07 ± 0.05	0.05 ± 0.01*	0.09 ± 0.02	0.08 ± 0.03

Notes. The peak area of the lipid $(CH_2)_n$ peak centered at 1.28 ppm was normalized to 1.00 in each spectrum, and the area of other peak in the same spectrum was scaled according to the lipid peak. The ppm range given in the leftmost column indicates the corresponding integral spectral range, i.e., terminal –C**H**$_3$ (0.7–1.4 ppm); –O–CO–CH$_2$–C**H**$_2$– (1.4–1.8 ppm); –CH=CH–C**H**$_2$–CH$_2$– (1.8–2.15 ppm); –O–CO–C**H**$_2$–CH$_2$– (2.15–2.4 ppm); –CH=CH–C**H**$_2$–CH=CH– (2.5–2.9 ppm); creatine (2.9–3.1 ppm); total cholines (choline, phosphocholine and phosphatidylcholine) (3.1–3.3 ppm); glycogen/glucose (3.3–3.5 ppm and 3.5–4.2 ppm); and C1, C3–glycerol ester (4.2–4.4 ppm), where the bold hydrogen in the notation corresponds to the NMR peak observed. Four animals were used in each group. Statistically significant differences between the exposed samples and the corresponding samples from aged-matched controls are indicated by * for $P \leq 0.05$ and ** for $P \leq 0.01$.

TABLE 1
Extended

Epiphysis + metaphysis of femur				
Control	3.0 Gy	7.8 Gy	Control	3.0 Gy
4	4	4	11	11
23.1 ± 4.6	23 ± 6.9	21.4 ± 4.6	27.5 ± 1.8	22.0 ± 3.5*
221 ± 64††	299 ± 95	4808 ± 188*	186 ± 30††	256 ± 41*
2522.3 ± 1308.3†	3723 ± 2043	5160 ± 768*	2280 ± 513††	2807 ± 663

the other peaks. This indicated that the epiphysis + metaphysis sections were more sensitive to radiation than the diaphysis of the same femurs. This conclusion was also supported by the results shown in Table 1 for the diaphysis; although both the weight-averaged total peak area and the peak area of long chain lipids $(CH_2)_n$ (1.1–1.4 ppm) were increased in the irradiated animals compared with their corresponding controls, the increase was not statistically significant. In contrast, a significant increase was observed for the corresponding epiphysis + metaphysis sections of the same femur.

DISCUSSION

Our results show that the levels of NMR-detectable metabolites in the epiphysis + metaphysis sections of mouse femurs were significantly higher than those in the diaphyses of the same femurs in the control and irradiated mice. Radiation caused greater damage to the metabolic profile in the epiphysis + metaphysis sections than to the diaphyses of the same femurs. This finding is not surprising because the femoral proximal metaphyses contain more hematopoietic cells than the epiphyses in adult animals (*9*). It is well known that the hematopoietic stem cells are both metabolically active and radiosensitive (*2–7*).

In the present study, we showed for the first time that ionizing radiation alters the lipid metabolism in bone marrow. The significantly increased level of NMR-detectable mobile fatty acids characterized by the long chain lipid $(CH_2)_n$ signal in the bone marrow of irradiated mice indicated that the fatty acids synthesis pathway is altered by radiation. Altered fatty acid biosynthesis, i.e., increased flux from glucose into fatty acids [the Warburg effect (*34, 35*)], has emerged as a feature of oncogenesis (*36, 37*). Increased mobile lipids

TABLE 2
Extended

Epiphysis + metaphysis				
Control	3 Gy	7.8 Gy	Control	3 Gy
4	4	4	11	11
0.20 ± 0.01	0.19 ± 0.006	0.18 ± 0.007*	0.22 ± 0.02	0.19 ± 0.004*
1.00 ± 0.35	1.00 ± 0.36	1.00 ± 0.40	1.00 ± 0.19	1.00 ± 0.18
0.16 ± 0.005	0.14 ± 0.013	0.14 ± 0.02	0.17 ± 0.01	0.15 ± 0.008**
0.19 ± 0.018	0.18 ± 0.004	0.17 ± 0.006*	0.22 ± 0.01	0.18 ± 0.004**
0.16 ± 0.008	0.15 ± 0.02	0.14 ± 0.004**	0.16 ± 0.01	0.15 ± 0.006**
0.067 ± 0.004	0.063 ± 0.007	0.063 ± 0.005	0.072 ± 0.006	0.067 ± 0.002
0.033 ± 0.0078	0.023 ± 0.004*	0.017 ± 0.004**	0.042 ± 0.008	0.027 ± 0.003**
0.097 ± 0.028	0.053 ± 0.01*	0.030 ± 0.011**	0.11 ± 0.019	0.065 ± 0.006**
0.034 ± 0.008	0.03 ± 0.016	0.016 ± 0.005**	0.045 ± 0.009	0.032 ± 0.005*
0.14 ± 0.04	0.11 ± 0.03	0.078 ± 0.020*	0.17 ± 0.03	0.11 ± 0.017*
0.048 ± 0.008	0.039 ± 0.008	0.037 ± 0.0046*	0.053 ± 0.0088	0.041 ± 0.0068

are often observed in proliferating cells and tumor cells and in the onset of apoptosis (*30, 38–42*). It is likely that the altered fatty acid synthesis after irradiation is one of the key biological pathways that predispose to cancer. However, more research is needed to validate this hypothesis.

The present study showed that the content of total choline (choline, PC and GPC) is decreased at the radiation doses studied. Phosphocholine is an important intermediate product in membrane choline phospholipids metabolism, where phosphatidylcholine and glycerophosphocholine are synthesized and hydrolyzed (*43*). Phosphatidylcholine is the most abundant phospholipid in biological membranes and together with other phospholipids, such as phosphatidylethanolamine and neutral lipids, forms the characteristic bilayer structure of cells and regulate membrane integrity (*44*). Prior studies have shown that altered phosphocholine and/or total choline levels are associated with malignancy (*43, 45, 46*). The significant decrease in total choline levels with increasing radiation dose indicates an altered membrane choline phospholipid metabolism. This is direct evidence that γ radiation causes measurable damage to the cell membrane.

SUMMARY

We demonstrated here that high-resolution MAS ^{1}H NMR can be used successfully to analyze the metabolites in intact bones from mice without the need for bone marrow extraction. The method is useful in profiling the pathology of bone marrow rapidly with minimal sample preparation. The spectral resolution allows several metabolites, including lipids, total choline (choline, phosphocholine, glycerophosphocholine), creatine, glycogen/glucose and glycerol esters, to be analyzed quantitatively. We found that the amounts of NMR-detectable metabolites in the epiphysis + metaphysis sections of mouse femur were significantly higher than those observed in the diaphysis of the same femur. We discovered that the major metabolite changes in the bone marrow after exposure to either 3 or 7.8 Gy of γ radiation, especially 4 days after exposure, were (1) decreased total choline content, (2) increased fatty acids in bone marrow, and (3) decreased creatine content. These results suggest that the fatty acid biosynthesis pathway and the membrane choline phospholipid metabolism (MCPM) pathway were altered in bone marrow after irradiation. This result is similar to those published recently on cell cycle arrest and death in carcinoma cells exposed to 20 Gy of γ radiation (*38*). The metabolites associated with these two basic molecular pathways, which were not known from prior studies (*47, 48*), are possible biomarkers characterizing radiation damage in bone marrow. These biomarkers, if validated, may serve as novel targets for medical countermeasures against ionizing radiation. Recently, a system-level metabolic flux profiling in cultured mammalian cells using liquid chromatography-tandem mass spectrometry has been used successfully to identify fatty acid synthesis as a target for antiviral therapy (*49*). Viral infection can contribute to the death after exposure to a lethal dose of ionizing radiation. We also found that the metabolic damage induced by radiation in the epiphysis + metaphysis sections of mouse femurs was higher than that of the diaphyses of the same femurs.

Traditional histopathology analysis was carried out in parallel to correlate histological damage with the metabolite changes. Histopathology revealed a mild depletion of hematopoietic cells in the bone marrow of the femurs at 4 days after exposure to 3 Gy radiation. By day 11 the bone marrow had returned to a normal histology. However, the bone marrow was severely depleted at 4 days after exposure to 7.8 Gy. The molecular information from high-resolution MAS ^{1}H NMR thus complements and expands the pathology data in a novel way. In particular, the significant changes in many metabolites found from high-resolution MAS ^{1}H NMR in the epiphysis + metaphysis sections 11 days after exposure to 3 Gy whole-body radiation suggest that metabolomics may be a more sensitive method for assessing radiation damage at this radiation dose. Therefore, it is reasonable to conclude that high-resolution MAS ^{1}H NMR is a powerful method for probing the pathology of radiation-induced damage at the molecular level. Essentially any kind of sample from an animal can be analyzed by this method because the analysis of intact bones represents the greatest challenge.

ACKNOWLEDGMENTS

This work was supported by the NASA Space Radiation Program under Grant NNX07AU44G and Pacific Northwest National Laboratory Directed Research and Development (LDRD) fund. All the NMR work was performed in the Environmental Molecular Sciences Laboratory (a National Scientific User Facility sponsored by the Department of Energy's Office of Biological and Environmental Research) located at PNNL, and operated for DOE by Battelle under Contract DE-AC05-76RL01830. RPP was supported in part by NIEHS grant ES01247 and by DE011390.

Received: January 14, 2009; accepted: July 8, 2009

REFERENCES

1. J. B. Tyburski, A. D. Patterson, K. W. Krausz, J. Slavik, A. J. Fornace, Jr., F. J. Gonzalez and J. R. Idle, Radiation metabolomics. 1. Identification of minimally invasive urine biomarkers for gamma-radiation exposure in mice. *Radiat. Res.* **170**, 1–14 (2008).
2. D. G. C. McCann, Radiation poisoning: Current concepts in the acute radiation syndrome. *Am. J. Clin. Med.* **3**, 13–21(2006).
3. N. Dainiak, Hematologic consequences of exposure to ionizing radiation. *Exp. Hematol.* **30**, 513–528 (2002).
4. T. M. Fliedner, D. Graessle, C. Paulsen and K. Reimers, Structure and function of bone marrow hemopoiesis: Mecha-

nisms of response to ionizing radiation exposure. *Cancer Biother. Radiopharm*. **17**, 405–426 (2002).

5. R. Coquard, Late effects of ionizing radiations on the bone marrow. *Cancer Radiother*. **1**, 792–800 (1997).
6. A. Banfi, G. Bianchi, M. Galotto, R. Cancedda and R. Quarto, Bone marrow stromal damage after chemo/radiotherapy: occurrence, consequences and possibilities of treatment. *Leuk. Lymphoma* **42**, 863–870 (2001).
7. T. M. Fliedner, D. Graessle, C. Paulsen and K. Reimers, Structure and function of bone marrow hemopoiesis: mechanisms of response to ionizing radiation exposure. *Cancer Biother. Radiopharm*. **17**, 405–426 (2002).
8. S. Hwang and D. M. Panicek, Magnetic resonance imaging of bone marrow in oncology, Part 2. *Skeletal Radiol*. **36**, 1017–1027 (2007).
9. S. Hwang and D. M. Panicek, Magnetic resonance imaging of bone marrow in oncology, Part 1. *Skeletal Radiol*. **36**, 913–920 (2007).
10. G. P. Schmidt, S. O. Schoenberg, M. F. Reiser and A. Baur-Melnyk, Whole-body MR imaging of bone marrow. *Eur. J. Radiol*. **55**, 33–40 (2005).
11. M. A. Tall, A. K. Thompson, T. Vertinsky and P. S. Palka, MR imaging of the spinal bone marrow. *Magn. Reson. Imaging Clin. N. Am*. **15**, 175–198 (2007).
12. D. K. Yeung, S. L. Lam, J. F. Griffith, A. B. Chan, Z. Chen, P. H. Tsang and P. C. Leung, Analysis of bone marrow fatty acid composition using high-resolution proton NMR spectroscopy. *Chem. Phys. Lipids* **151**,103–109 (2008).
13. S. Muthusami, I. Ramachandran, B. Muthusamy, G. Vasudevan, V. Prabhu, V. Subramaniam, A. Jagadeesan and S. Narasimhan, Ovariectomy induces oxidative stress and impairs bone antioxidant system in adult rats. *Clin. Chim. Acta* **360**, 81–86 (2005).
14. P. Weybright, K. Millis, N. Campbell, D. G. Cory and S. Singer, Gradient, high-resolution, magic angle spinning ^{1}H nuclear magnetic resonance spectroscopy of intact cells. *Magn. Reson. Med*. **39**, 337–345 (1998).
15. R. A. Wind, J. Z. Hu and D. N. Rommereim, High-resolution ^{1}H NMR spectroscopy in organs and tissues using slow magic angle spinning. *Magn. Reson. Med*. **46**, 213–218 (2001).
16. L. L. Cheng, M. J. Ma, L. Becerra, T. Ptak, I. Tracey, A. Lackner and R. G. Gonzalez, Quantitative neuropathology by high resolution magic angle spinning proton magnetic resonance spectroscopy. *Proc. Natl. Acad. Sci. USA* **94**, 6408–6413 (1997).
17. J. Z. Hu, D. N. Rommereim, K. R. Minard, A. Woodstock, B. J. Harrer, R. A. Wind, R. P. Phillips and P. J. Sime, Metabolomics in lung inflammation: A high-resolution ^{1}H NMR study of mice exposed to silica dust. *Toxicol. Mech. Methods* **18**, 385–398 (2008).
18. M. E. Bollard, A. J. Murray, K. Clarke, J. K. Nicholson and J. L. Griffin, A study of metabolic compartmentation in the rat heart and cardiac mitochondria using high-resolution magic angle spinning ^{1}H NMR spectroscopy. *FEBS Lett*. **553**, 73–78 (2003).
19. A. R. Tate, P. J. Foxall, E. Holmes, D. Moka, M. Spraul, J. K. Nicholson and J. C. Lindon, Distinction between normal and renal cell carcinoma kidney cortical biopsy samples using pattern recognition of ^{1}H magic angle spinning (MAS) NMR spectra. *NMR Biomed*. **13**, 64–71 (2000).
20. V. Righi, A. Mucci, L. Schenetti, M. R. Tosi, W. F. Grigioni, B. Corti, A. Bertaccini, A. Franceschelli, F. Sanguedolce and V. Tugnoli, Ex vivo HR-MAS magnetic resonance spectroscopy of normal and malignant human renal tissues. *Anticancer Res*. **27**, 3195–3204 (2007).
21. J. H. Chen, Y. V. Wu, P. Decarolis, R. O'Connor, C. J. Somberg and S. Singer, Resolution of creatine and phosphocreatine ^{1}H signals in isolated human skeletal muscle using HR-MAS ^{1}H NMR. *Magn. Reson. Med*. **59**, 1221–1224 (2008).
22. M. E. Bollard, S. Garrod, E. Holmes, J. C. Lindon, E. Humpfer, M. Spraul and J. K. Nicholson, High-resolution ^{1}H and ^{1}H-^{13}C magic angle spinning NMR spectroscopy of rat liver. *Magn. Reson. Med*. **44**, 201–207 (2000).
23. S. Garrod, E. Humpfer, M. Spraul, S. C. Connor, S. Polley, J. Connelly, J. C. Lindon, J. K. Nicholson and E. Holmes, High-resolution magic angle spinning ^{1}H NMR spectroscopic studies on intact rat renal cortex and medulla. *Magn. Reson. Med*. **41**, 1108–1118 (1999).
24. S. Garrod, E. Humpher, S. C. Connor, J. C. Connelly, M. Spraul, J. K. Nicholson and E. Holmes, High-resolution ^{1}H NMR and magic angle spinning NMR spectroscopic investigation of the biochemical effects of 2-bromoethanamine in intact renal and hepatic tissue. *Magn. Reson. Med*. **45**, 781–790 (2001).
25. Y. F. Zhou, M. Bosch-Marce, H. Okuyama, B. Krishnamachary, H. Kimura, L. Zhang, D. L. Huso and G. L. Semenza, Spontaneous transformation of cultured mouse bone marrow-derived stromal cells. *Cancer Res*. **66**, 10849–10854 (2006).
26. N. C. Peterson, M. D. Servinsky, A. Christian, Z. Peng, W. Qiu, J. Mann, J. Dicello and D. L. Huso, Tamoxifen resistance and Her2/neu expression in an aged, irradiated rat breast carcinoma model. *Carcinogenesis* **26**, 1542–1552 (2005).
27. G. Morris and R. Freeman, Selective excitation in Fourier transform nuclear magnetic resonance. *J. Magn. Reson*. **29**, 433–462 (1978).
28. R. J. Barlow, *Statistics: A Guide to the Use of Statistical Methods in the Physical Sciences*, pp. 159–160. Wiley, Chichester, 1989.
29. J. L. Griffin, C. J. Mann, J. Scott, C. C. Shoulders and J. K. Nicholson, Choline containing metabolites during cell transfection: an insight into magnetic resonance spectroscopy detectable changes. *FEBS Lett*. **509**, 263–266 (2001).
30. A. Rosi, A. Luciani, P. Matarrese, G. Arancia, V. Viti and L. Guidoni, ^{1}H-MRS lipid signal modulation and morphological and ultrastructural changes related to tumor cell proliferation. *Magn. Reson. Med*. **42**, 248–257 (1999).
31. H. Bays, L. Mandarino and R. A. DeFronzo, Role of the adipocyte, free fatty acids, and ectopic fat in pathogenesis of type 2 diabetes mellitus: peroxisomal proliferator-activated receptor agonists provide a rational therapeutic approach. *J. Clin. Endocrinol. Metab*. **89**, 463–478 (2004).
32. H. J. Atherton, N. J. Bailey, W. Zhang, J. Taylor, H. Major, J. Shockcor, K. Clarke and J. L. Griffin, A combined ^{1}H-NMR spectroscopy- and mass spectrometry-based metabolomic study of the PPAR-alpha null mutant mouse defines profound systemic changes in metabolism linked to the metabolic syndrome. *Physiol. Genomics* **27**, 178–186 (2006).
33. M. Borkman, L. H. Storlien, D. A. Pan, A. B. Jenkins, D. J. Chisholm and L. V. Campbell, The relation between insulin sensitivity and the fatty-acid composition of skeletal-muscle phospholipids. *N. Engl. J. Med*. **328**, 238–244 (1993).
34. O. Warburg, *The Metabolism of Tumors*. Constable, London, 1930.
35. O. Warburg, On the origin of cancer cells. *Science* **123**, 309–314 (1956).
36. D. E. Bauer, G. Hatzivassiliou, F. Zhao, C. Andreadis and C. B. Thompson, ATP citrate lyase is an important component of cell growth and transformation. *Oncogene* **24**, 6314–6322 (2005).
37. C. D. Young and S. M. Anderson, Sugar and fat—that's where it's at: metabolic changes in tumors. *Breast Cancer Res*. **10**, 202 (2008).
38. A. M. Luciani, S. Grande, A. Palma, A. Rosi, C. Giovannini, O. Sapora, V. Viti and L. Guidoni, Characterization of H-1 NMR detectable mobile lipids in cells from human adeno-carcinomas. *FEBS J*. **276**, 1333–1346 (2009).
39. J. M. Hakumaki and R. A. Kauppinen, ^{1}H NMR visible lipids in the life and death of cells. *Trends Biochem. Sci*. **25**, 357–362 (2000).
40. E. J. Delikatny, C. M. Lander, T. M. Jeitner, R. Hancock and C. E. Mountford, Modulation of MR-visible mobile lipid levels

by cell culture conditions and correlations with chemotactic response. *Int. J. Cancer* **65**, 238–245 (1996).

41. J. M. Hakumaki and T. Liimatainen, Molecular imaging of apoptosis in cancer. *Eur. J. Radiol*. **56**, 143–153 (2005).

42. M. Milkevitch, H. Shim, U. Pilatus, S. Pickup, J. P. Wehrle, D. Samid, H. Poptani, J. D. Glickson and E. J. Delikatny, Increases in NMR-visible lipid and glycerophosphocholine during phenylbutyrate-induced apoptosis in human prostate cancer cells. *Biochim. Biophys. Acta* **1734**, 1–12 (2005).

43. E. O. Aboagye and Z. M. Bhujwalla, Malignant transformation alters membrane choline phospholipid metabolism of human mammary epithelial cells. *Cancer Res*. **59**, 80–84 (1999).

44. C. E. Mountford and L. C. Wright, Organization of lipids in the plasma membranes of malignant and stimulated cells: a new model. *Trends Biochem. Sci*. **13**, 172–177 (1988).

45. J. Ruiz-Cabello and J. S. Cohen, Phospholipid metabolites as indicators of cancer cell function. *NMR Biomed*. **5**, 226–233 (1992).

46. W. B. Mackinnon, P. A. Barry, P. L. Malycha, D. J. Gillett, P. Russell, C. L. Lean, S. T. Doran, B. H. Barraclough, M. Bilous and C. E. Mountford, Fine-needle biopsy specimens of benign breast lesions distinguished from invasive cancer ex vivo with proton MR spectroscopy. *Radiology* **204**, 661–666 (1997).

47. S. Grande, C. Giovannini, L. Guidoni, A. M. Luciani, A. Palma, A. Rosi, O. Sapora and V. Viti, ^{1}H MRS signals from glutathione may act as predictive markers of apoptosis in irradiated tumour cells. *Radiat. Prot. Dosimetry* **122**, 205–206 (2006).

48. A. D. Patterson, H. Li, G. S. Eichler, K. W. Krausz, J. N. Weinstein, A. J. Fornace, Jr., F. J. Gonzalez and J. R. Idle, UPLC-ESI-TOFMS-based metabolomics and gene expression dynamics inspector self-organizing metabolomic maps as tools for understanding the cellular response to ionizing radiation. *Anal. Chem*. **80**, 665–674 (2008).

49. J. Munger, B. D. Bennett, A. Parikh, X. Feng, J. McArdle, H. A. Rabitz, T. Shenk and J. D. Rabinowitz, Systems-level metabolic flux profiling identifies fatty acid synthesis as a target for antiviral therapy. *Nat. Biotechnol*. **26**, 1179–1186 (2008).